Supplementary Information for

Orientation of a Diagnostic Ligand Bound to Macroscopically-Aligned Amyloid-β Fibrils Determined by Solid-state NMR

David Townsend, Eleri Hughes, Katie L. Stewart, John M. Griffin, Sheena E. Radford and David A. Middleton*

Contents:

1. Experimental details

1.1 Expression and purification of MAβ40

Commercial *Escherichia coli* strain BL21 (DE3) cells (Agilent) were transformed with a pETSAC plasmid containing the sequence for Aβ40 [1] and bacteria were grown in MEM (minimal medium with 2 g/L ^{13}C glucose and 1 g/L ^{15}N ammonium chloride) [1-2]. Cultures were grown and Aβ40 purified as described previously [2-3]. The resulting sequence contains an additional N-terminal methionine residue that has no effect on the fibrillation of Aβ40 or the morphology of fibrils formed.[1] Final protein concentrations were estimated from UV absorption in 7 M guanidinium chloride at 280 nm using an extinction coefficient of 1490 M^{-1} cm^{-1}.

1.2 Aβ40 3Q fibril preparation

3Q fibrils of Aβ40 were prepared by diluting fibrils of the 3Q morphology [4] (a gift from R. Tycko) to 5% (v/v) in seeding buffer (25 mM NaH_2PO_4, pH 7.5, 0.01% (w/v) NaN_3) and sonicating for 5 s followed by 45 s rest for 3 cycles at amplitude 20% (approx. 3 J) to produce seeds. Lyophilized monomeric Aβ40 was added to the fibril seeds to a concentration of 0.9 mg/mL and incubated quiescently overnight at 25 °C in 2.5 mL centrifuge tubes. After 18 h, the fibrils were sonicated for 5 s, and incubated quiescently at 25 ^{0}C for one week. Fibril growth was verified by negative stain TEM.

1.3 Analysis of FSB binding to fibrils

For analysis by UV/Vis spectroscopy, FSB (0-450 μM) in 100 μL 25 mM phosphate buffer, 0.1% NaN_3, pH 7.5 was agitated alone or with 45 μM Aβ40 fibrils (3Q seeded) at 37℃ overnight. The suspension was centrifuged at 13,400 rpm on a b enchtop centrifuge. Absorbance of the supernatant was recorded on a Flexstation 3 Multiplate Reader (Molecular Devices) between 200-600 nm. For fluorescence measurements, FSB (47 μM and 23 μM) was incubated alone or in the presence of 45 μM Aβ40 fibrils overnight at 37℃ with shaking. The insoluble material was removed through centrifugation at 13,400 rpm on a benchtop centrifuge. A Flexstation 3 Multiplate Reader (Molecular devices) was used to measure the absorbance of the supernatant between 200-700 nm, and the fluorescence between 380-700 nm with excitation at 360 nm. All samples were analysed in triplicate and the means and standard errors are reported.

1.4 Preparation of oriented fibrils

3Q-seeded fibrils of [U-^{15}N,^{13}C]Aβ40 (5 mg protein) were incubated with a 2-fold molar excess of FSB overnight and then subjected to two centrifugation/resuspension cycles to remove any excess unbound FSB. The washed fibrils were suspended to 1.3 % in 25 mM NaH_2PO_4 and deposited on 25 glass cover slips (Paul Marienfeld GmbH & Co. KG, Gemany; 8 x 22 mm, thickness No. 0 (0.08-0.12mm)) that had been pre-sonicated in MeOH followed by rinsing in EtOH then MilliQ grade water, in a series of 20 µl repeated aliquots to ensure even coverage across the glass. The cover slips were allowed to dry under ambient conditions for 48 h and then incubated for a further 24 h under constant humidity (60 %). The cover slips were stacked and wrapped in cling film immediately before NMR analysis.

1.5 NMR analysis

All measurements were performed on a Bruker Avance III spectrometer with an 89 mm bore magnet operating at 9.3 T. The REDOR spectra, the ^{1}H,^{15}N- polarization-inversion spin-exchange at the magic-angle (PISEMA) spectrum of unoriented fibrils and the ^{19}F spectrum of unoriented FSB (i.e., the solid material and FSB bound to randomly-dispersed fibrils) were acquired with a Bruker 3.2 mm quadruple resonance (HFXY) magic-angle spinning probe. Measurements on the aligned fibrils were performed with a static, double resonance (H/F and X) flat-coil probe (Bruker) with coil dimensions 9 x 9 x 3 mm.

The ^{19}F spectra of solid FSB and FSB bound to randomly-dispersed fibrils were obtained with an initial 2.5 μs 90° pulse at the frequency of ^{1}H followed by 2-ms ramped cross-polarisation from ^{1}H to ^{19}F at a proton field of 40 kHz. Proton decoupling was applied during signal acquisition with SPINAL-64 [5] at a proton field of 83 kHz. The same procedure was followed for the proton-coupled spectrum except that the ^{1}H transmitter was turned off during signal acquisition. The ^{19}F spectra of the fibril sample were the result of averaging 20,480 transients and the spectrum of solid FSB is the result of averaging 128 transients.

For the ^{13}C{^{19}F}REDOR experiment, an initial 2.5 μs 90° pulse at the frequency of ^{1}H was followed by 2-ms ramped cross-polarization Hartmann-Hahn from ^{1}H to ^{13}C over a 2-ms contact time with a ramped proton spin-lock field centred

at 60 kHz. The recycle delay was 2 s. The full spin-echo ^{13}C spectrum without ^{19}F dephasing was obtained at a magic-angle spinning (MAS) frequency of 6 kHz, and a dephasing/echo time of 3.5 ms. A train of 21 π pulses at the ^{19}F frequency was applied during the echo period to obtain the dephased echo spectrum. A difference spectrum corresponding to the dephased peaks was obtained by subtracting the dephased-echo spectrum from the full-echo spectrum. REDOR measurements were performed at -20℃ to reduce molecular dynamics that may otherwise scale weak dipolar couplings. SPINAL-64 decoupling at a field of 83 kHz was applied during the echo period and signal acquisition. The full-echo and dephased-echo spectra were each obtained by averaging 10,240 transients.

The ^{1}H-^{19}F PISEMA spectrum of solid FSB was obtained using the basic pulse sequence described by Wu et al.[6] For the lyophilised sample, an initial 2.5 μs 90° pulse on ^{1}H was followed by 2 ms ramped cross-polarisation from ^{1}H to ^{19}F at a proton nutation frequency of 40 kHz. Spin exchange at the magic-angle was achieved using frequency-switched Lee-Goldberg cross-polarization at a proton field of 62.5 kHz and matched ^{19}F field of 76 kHz. Proton decoupling at a field of 62.5 kHz was applied during signal acquisition The spectrum was the result of 32 t_1 increments in the indirect dimension, with averaging of 512 transients per increment.

For the ^{1}H-^{15}N PISEMA spectra of the aligned and randomly-dispersed fibrils, an initial 2.5 μs 90° pulse on ^{1}H was followed by 2 ms ramped cross-polarization from ^{1}H to ^{15}N at a proton nutation frequency of 40 kHz. Frequency-switched Lee-Goldberg cross-polarisation was applied at a proton field of 62.5 kHz and matched ^{15}N field of 76 kHz and 62.5 kHz proton decoupling was applied during signal acquisition. The spectra were the result of 32 t_1 increments in the indirect dimension, with averaging of 512 transients per increment.

The proton-coupled 1D ^{19}F spectrum of the oriented FSB:[U-^{13}C,^{15}N]Aβ40 fibril complex was obtained using the DEPTH method[7] with a ^{19}F $\pi/2$ pulse length of 3.5 μs to eliminate any background signal from ^{19}F outside of the coil. The spectrum was obtained by averaging 102,400 transients in 10 blocks of 10,240, with a recycle delay of 3 s.

1.6 Calculation of the ^{19}F chemical shift tensor elements of FSB

First principles calculations on an isolated, optimized FSB molecule were performed to predict the orientation of the ^{19}F chemical shift principal axes, $\hat{\delta}_{11}$, $\hat{\delta}_{22}$ and $\hat{\delta}_{33}$, in the molecular frame and the corresponding principal values, δ_{11}, δ_{22} and δ_{33}. This information is required to determine the molecular orientation of FSB relative to the fibril axis (**see Section 1.8**). Optimization of the FSB molecular geometry and calculation of the NMR parameters was performed using the CASTEP density functional theory code,[8] employing the GIPAW algorithm,[9] which allows the reconstruction of the all-electron wave function in the presence of a magnetic field. The CASTEP calculations employed the generalised gradient approximation (GGA) PBE functional[10] and core–valence interactions were described by ultrasoft pseudopotentials.[11] In the geometry optimizations for the single molecule and for the crystal structure, all atomic positions were allowed to vary. The optimisation of the methanol solvate crystal structure was carried out using the G06 semi-empirical dispersion correction scheme,[12] with the unit cell parameters allowed to vary. Both the geometry optimisation and NMR calculation for this structure were carried out with a k-point spacing of 0.05 2π Å^{-1} and a planewave energy cut-off of 50 Ry. For the isolated molecule, the geometry optimisation and NMR calculation were performed by placing the molecule in a 25 Å x 25 Å x 20 Å cell. These calculations were also performed using a planewave energy cut-off of 50 Ry (680 eV) but due to the large cell size, a single k-point at the fractional coordinate (0.25, 0.25, 0.25) in reciprocal space for integration over the Brillouin zone. The calculations generate the absolute shielding tensor ($\boldsymbol{\sigma}$) and diagonalization of the symmetric part of $\boldsymbol{\sigma}$ yields as eigenvalues the principal components σ_{XX}, σ_{YY} and σ_{ZZ} and their orientations in the molecular frame are given by the eigenvectors. By definition σ_{ZZ} is the most shielded calculated component and σ_{XX} is the least shielded. Finally, the shielding components are converted to chemical shifts by subtracting σ_{11}, σ_{22} and σ_{33} from a single reference value, σ_{ref}, to give δ_{11}, δ_{22} and δ_{33} and their corresponding principal axes $\hat{\delta}_{11}$, $\hat{\delta}_{22}$ and $\hat{\delta}_{33}$.

Using this approach, $\hat{\delta}_{22}$ is calculated to be to be directed along the C-F bond and the most shielded component ($\hat{\delta}_{11}$) is normal to the plane of the fluorophenyl ring (Figure S5a). Calculated principal values are close to the values measured from the

static proton-decoupled ^{19}F NMR spectrum of FSB powder (Table S1 and Figure S5b).

1.7 Experimental verification of the FSB ^{19}F CSA tensor orientation

The directions of the three orthogonal principal axes, $\hat{\delta}_{11}$, $\hat{\delta}_{22}$ and $\hat{\delta}_{33}$, of the ^{19}F chemical shift tensor in the FSB molecular frame were analysed using the ^{1}H-^{19}F PISEMA NMR method described recently.[13] The PISEMA spectrum correlates the ^{19}F CSA of solid FSB with dipolar couplings between ^{19}F and neighbouring protons occupying known positions relative to fluorine in the conjugated planar molecule. The PISEMA spectrum of solid FSB was compared with a series of simulated spectra for different ^{19}F CSA tensor orientations in the molecular frame. Simulated spectra were calculated in the SIMPSON programming environment using the standard SIMPSON script with crystallite file zcw4180[14] modified to include specific NMR parameters calculated from the optimised, lowest-energy FSB structure. These parameters represented a 4 spin system (1 x ^{19}F and 3 x ^{1}H) as illustrated in Figure S5c, where the three protons are those closest in space to fluorine in the optimised structure. Contributions of the remaining protons to the spectrum were insignificant. The FSB-specific parameters are the four ^{1}H-^{19}F dipolar coupling constants, measured chemical shift elements and the Euler angles α_{DC}, β_{CD} and γ_{DC} defining the orientations of each ^{1}H-^{19}F dipolar vector i in the ^{19}F chemical shift reference frame. Hence in the simulations for different ^{19}F tensor orientations, the only variables are α_{DC}, β_{CD} and γ_{DC}.

Figure S5c shows the experimental ^{1}H-^{19}F PISEMA NMR spectrum of solid FSB superimposed with a simulated spectrum in which the ^{19}F CSA tensor is oriented as predicted by CASTEP (i.e., with $\hat{\delta}_{22}$ directed along the C-F bond and $\hat{\delta}_{11}$ normal to the plane of the fluorophenyl ring). Figure S6 indicates that there is significant mismatch between experimental and simulated spectra for tensor orientations, with $\hat{\delta}_{11}$ or $\hat{\delta}_{33}$ along the C-F bond. Hence the CASTEP predicted geometry was considered to be correct and used as the basis for the further calculations.

1.8 Simulation of ^{19}F NMR spectra

A theoretical framework was developed to predict the ^{19}F NMR spectrum for any specific orientation of FSB relative to the fibril axis in the aligned FSB-[U-

^{15}N,^{13}C]Aβ40 complex. It was assumed that the fibrils were tilted at 90° with respect to B_0 and distributed cylindrically about the fibril long axis; in other words, across the population of aligned fibrils any external face of each fibril could contact the planar substrate surface with equal probability. Consequently, FSB molecules bound to the fibril with a unique orientation relative to the fibril axis are also distributed cylindrically across the fibril population. The ^{19}F NMR line shape is dependent on the orientations of the principal axes of the ^{19}F chemical shift tensor, $\hat{\delta}_{11}$, $\hat{\delta}_{22}$ and $\hat{\delta}_{33}$, relative to the fibril long axis, defined by angles α_{CF} and β_{CF} (Figure S7a). These angles remain invariant if the ligand crystallites are rotated about the fibril axis (Figure S7b). However, angles α_{CL} and β_{CL}, which define the orientations of the principal axes in a laboratory frame with B_0 along the z-axis, assume a continuum of values as a result of the rotational operation (Figure S7, c and d) and this distribution of values determines the line shape of the ^{19}F spectrum (Figure S7e). In order to translate the NMR line shape into the ligand orientation relative to the fibrils it is necessary to know the directions of $\hat{\delta}_{11}$, $\hat{\delta}_{22}$ and $\hat{\delta}_{33}$ relative to the FSB molecular geometry. DFT calculations supported by ^{19}F NMR measurements (**see sections 1.6 and 1.7 for details**) indicate that $\hat{\delta}_{22}$ is directed along the C-F bond and $\hat{\delta}_{11}$ normal to the plane of the fluorophenyl ring).

As ^{19}F could not be observed with proton decoupling in our rectangular-coil probe, ^{1}H-^{19}F dipolar couplings as well as the ^{19}F CSA must be considered in the simulations. Simulated 1D proton-coupled ^{19}F NMR spectra of oriented FSB were based on the 4-spin (1 x ^{19}F and 3 x ^{1}H) system (as shown in Figure 5c) for which the ^{1}H-^{19}F dipolar couplings and Euler angles defining the orientation of the ^{1}H-^{19}F dipolar vectors in the ^{19}F chemical shift frame were calculated from the optimised geometry of FSB. The simulations also required the values of the ^{19}F CSA tensor elements, which were measured directly from the proton-decoupled ^{19}F NMR spectrum of FSB bound to the unoriented fibrils (Table 1 and Figure 4a of the main text). A C programme was written to calculate the angles α_{CL} and β_{CL} defining the orientations of the cylindrically-distributed ^{19}F CSA tensors in a laboratory frame with the z-axis parallel with B_0. Angles representing a distribution of 360 crystallites were calculated for each combination of the angles α_{CF} and β_{CF}, which define the orientation of the ^{19}F CSA tensor relative to the fibril long axis. The fibril axis was assumed to be perpendicular to B_0. The list of angles α_{CL} and β_{CL} were written to a

crystallite file used by SIMPSON to simulate a spectrum for each combination of α_{CF} and β_{CF}. Finally, both angles α_{CF} and β_{CF} were varied in 15° increments from 0° to 180°, resulting in 144 simulated spectra. These were each compared with the experimental ^{19}F spectrum of the oriented sample to obtain the χ^2 values shown in the contour plot in Figure S8.

1.9 Molecular docking simulations

Docking simulations were carried out using Molsoft ICM-Pro V3.8 with the structural model for $A\beta_{1-40}$ in the three-fold molecular symmetry (3Q) morphology (PDB 2LMP) and the optimized structure for FSB imported from chEMBL. Three regions were selected for docking, guided by the amino acid-FSB contacts identified in the REDOR experiment (Figure 1d and Figure S9). Docking runs were performed with the histidines, prolines, asparagines, glutamines and cysteines optimised, and water molecules restricted to tight conformations, through the conversion of the pdb file in ICM-Pro. Each docking run had a thoroughness limit of 10, and generated the top 20 conformations in terms of energy (kcal/mol), reported as a dimensionless ICM Pro score. Generally a score below -32 is regarded as a good docking score, and the top ten docking structures presented in Figure 4c scored between -50.1 and -32.1.

2. Tabulated data

Table S1. Experimental and calculated ^{19}F static chemical shift tensor elements for FBTA. The values of the principal components follow the Haeberlen convention $|\delta_{11} - \delta_{iso}| \geq |\delta_{33} - \delta_{iso}| \geq |\delta_{22} - \delta_{iso}|$, where the isotropic chemical shift $\delta_{iso} = (\delta_{11} + \delta_{22} + \delta_{33})/3$. The anisotropy $\Delta\delta = 3(\delta_{11}-\delta_{iso})/2$ and the asymmetry parameter $\eta = (\delta_{22} - \delta_{33})/(\delta_{11} - \delta_{iso})$. Calculated principal values were obtained from the computed shielding tensor elements and are defined as $\delta_{11} = \sigma_{ref} - \sigma_{ZZ}$, $\delta_{22} = \sigma_{ref} - \sigma_{YY}$ and $\delta_{33} = \sigma_{ref} - \sigma_{XX.}$, where σ_{ZZ} is the most shielded calculated component and σ_{XX} is the least shielded. The reference value $\sigma_{ref} = \delta_{iso} - \sigma_{iso}$, where $\sigma_{iso} = (\sigma_{XX} + \sigma_{YY} + \sigma_{ZZ})/3$ and δ_{iso} is the measured value for solid FSB.

	δ_{11} (ppm)	δ_{22} (ppm)	δ_{33} (ppm)	$\Delta\delta$ (ppm)	η	δ_i (ppm)
FSB (solid)	-195.1	-110.7	-47.8	-77.3	0.81	-118.2
FSB (fibril)	-188.6	-108.2	-49.8	-73.1	0.80	-115.5
FSB (DFT)	-220.2	-103.2	-31.2	-102.0	0.71	-118.2

Table S2. Docking scores (dimensionless) from ICM-Pro corresponding to the 10 lowest-energy models shown in Figure 4c and Figure S9.

Model	Overall score	Intermolecular contributions		
		H-bond	Hydrophobic	WdW
1	-50.1	-7.1	-6.7	-29.9
2	-48.3	-7.4	-5.9	-27.1
3	-47.01	-8.4	-6.2	-28.2
4	-46.0	-9.2	-6.5	-25.4
5	-41.6	-5.8	-6.2	-29.5
6	-41.3	-5.1	-6.6	-29.7
7	-36.8	-3.1	-5.8	-30.8
8	-36.5	-3.1	-5.6	-31.0
9	-35.6	-3.7	-6.5	-33.9
10	-32.1	-3.1	-4.6	-23.6

3. Supplementary Figures

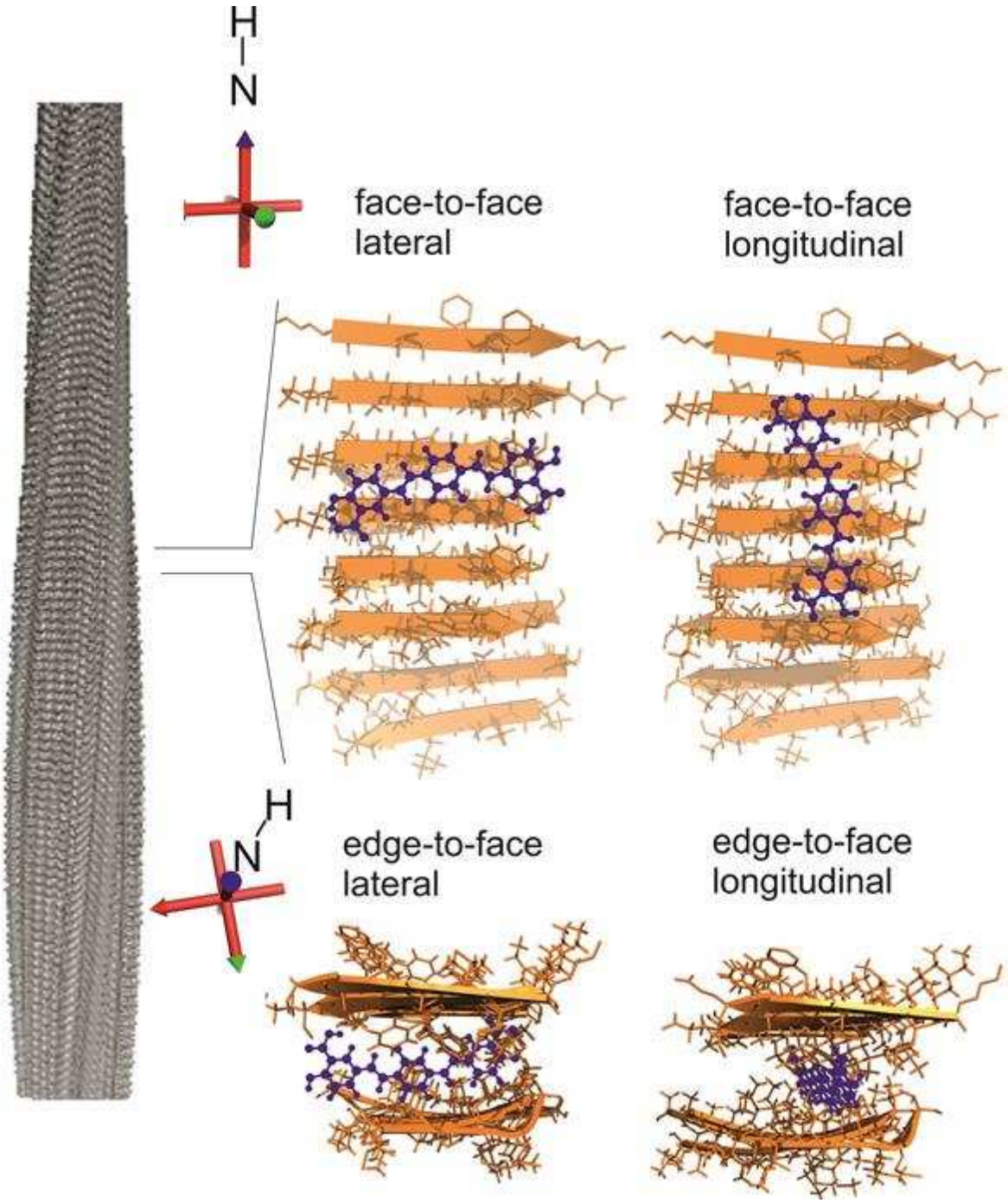

Figure S1. Examples of different possible orientations of a ligand molecule bound to the amyloid cross-β architecture externally (top) or between β-sheet layers (bottom).

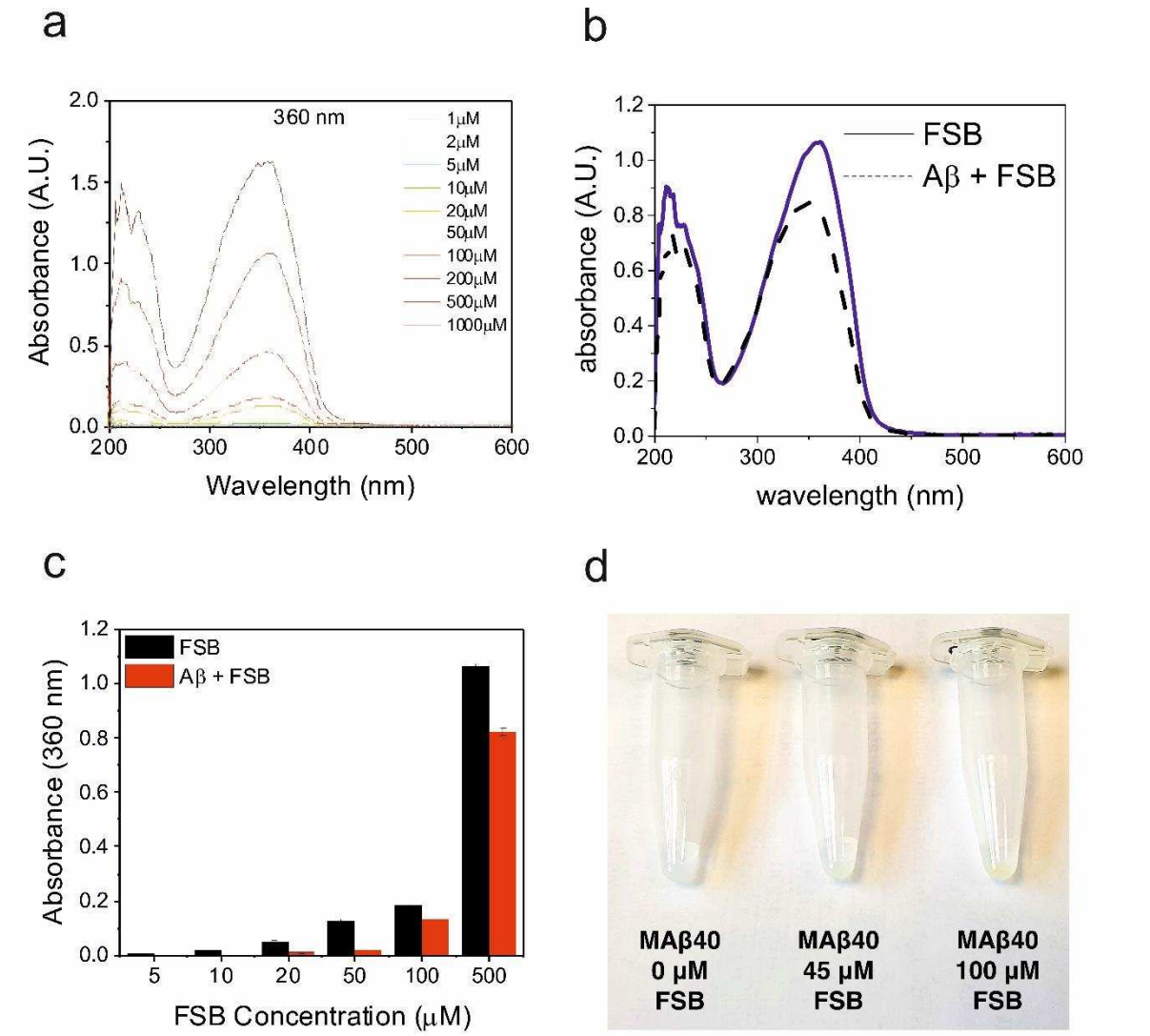

Figure S2. Measurements of the interaction between FSB and Aβ40 fibrils. (a) FSB concentration dependence of the absorbance in aqueous solution. (b) Absorbance of 500 μM FSB in solution alone (black) and after addition of Aβ40 fibrils (45 μM) and removal of the insoluble material by centrifugation (red). (c) Concentration-dependence of FSB binding to Aβ40 fibrils from the absorbance at 360 nm (λ_{max}). (d) The insoluble pellet after centrifugation viewed under a UV lamp.

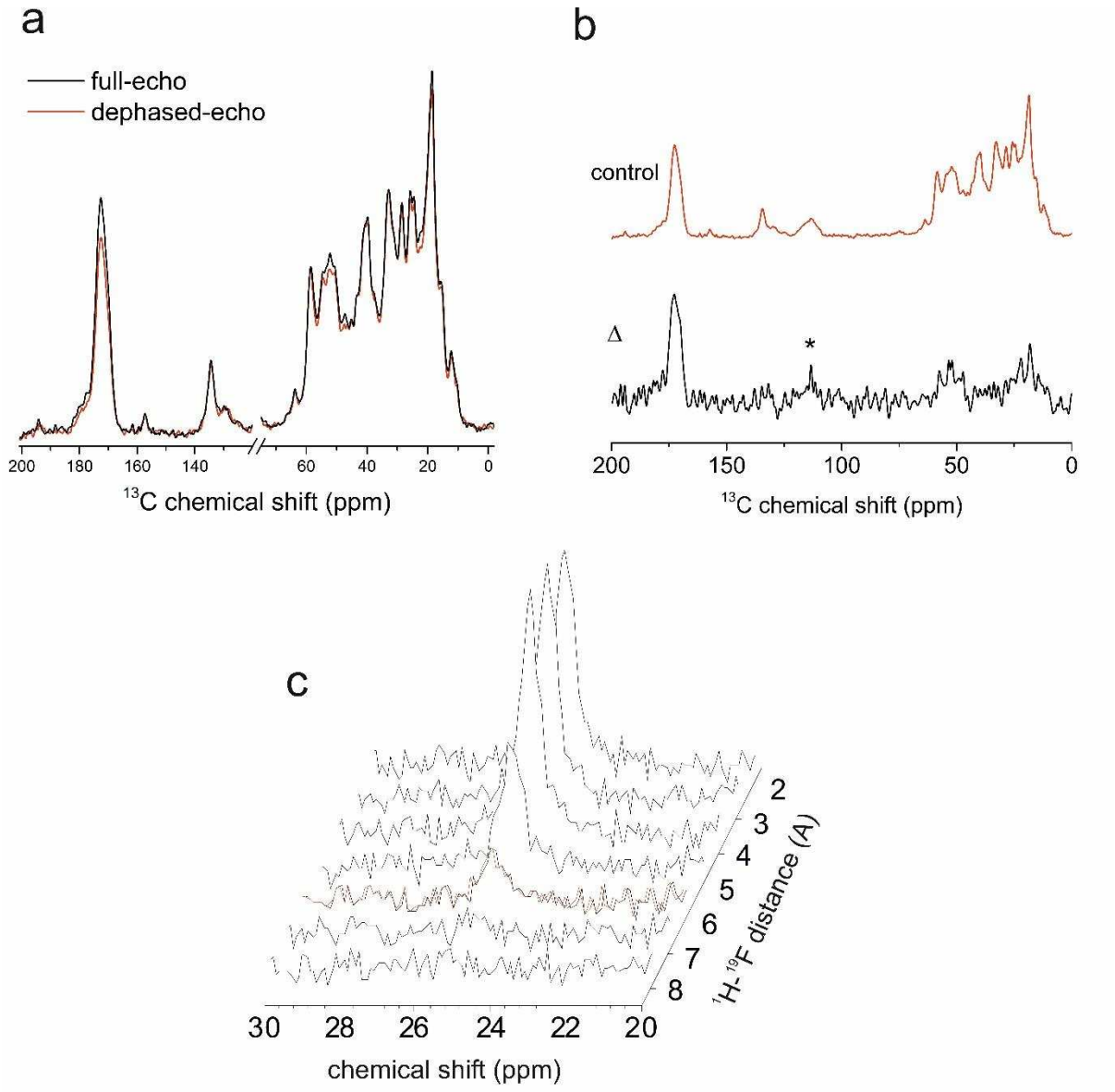

Figure S3. $^{13}C\{^{19}F\}$REDOR NMR spectra reproduced in full from the main text. (a) The full-echo spectrum overlaid with the dephased-echo spectrum to highlight the regions of selective dephasing. (b) Comparison of the control, full-echo spectrum with the difference spectrum (Δ) obtained by subtraction of the dephased-echo spectrum from the control spectrum. (c) Simulated $^{13}C\{^{19}F\}$REDOR difference spectra at a dephasing time of 3.5 ms to illustrate the limit of detection of dephasing at a signal-to-noise ratio (SNR) of 10:1. The intensities of the difference spectra reflect the extent of dipolar dephasing, which is inversely proportional to the cube of the internuclear distance. ^{13}C-^{19}F distances of up to 6 Å (highlighted in red) give rise to detectable dephasing of the ^{13}C signal at this SNR.

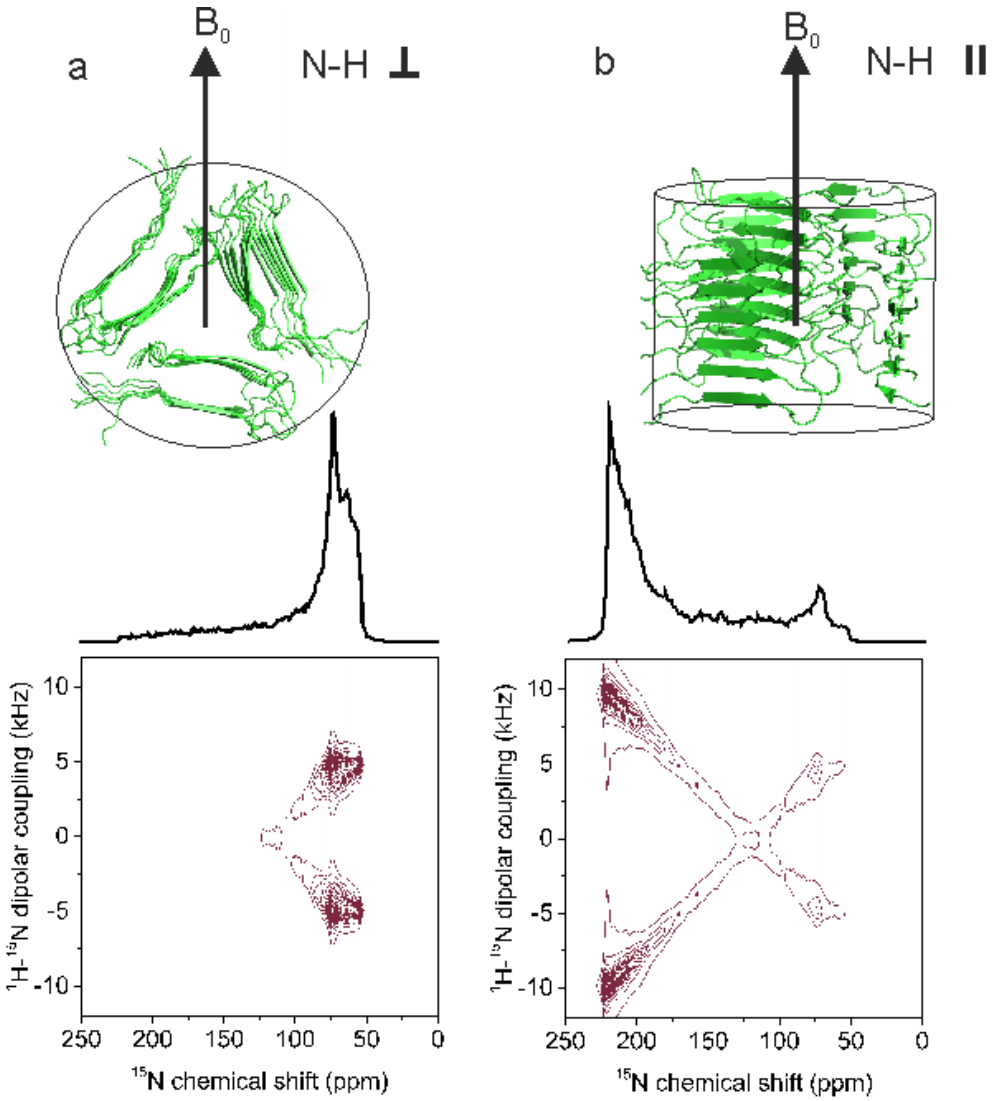

Figure S4. Simulated $^{1}H,^{15}N$-PISEMA spectra for Aβ40 fibrils in the 3Q geometry (taken from the model in the PDB file 2LMP). The model was rotated with the symmetry axis (and hence the approximate backbone N-H bond orientations) either perpendicular to or parallel with B_0. The atomic coordinates in the PDB file were then extracted to calculate the chemical shift and ^{1}H-^{15}N dipolar coupling for each amino acid residue.

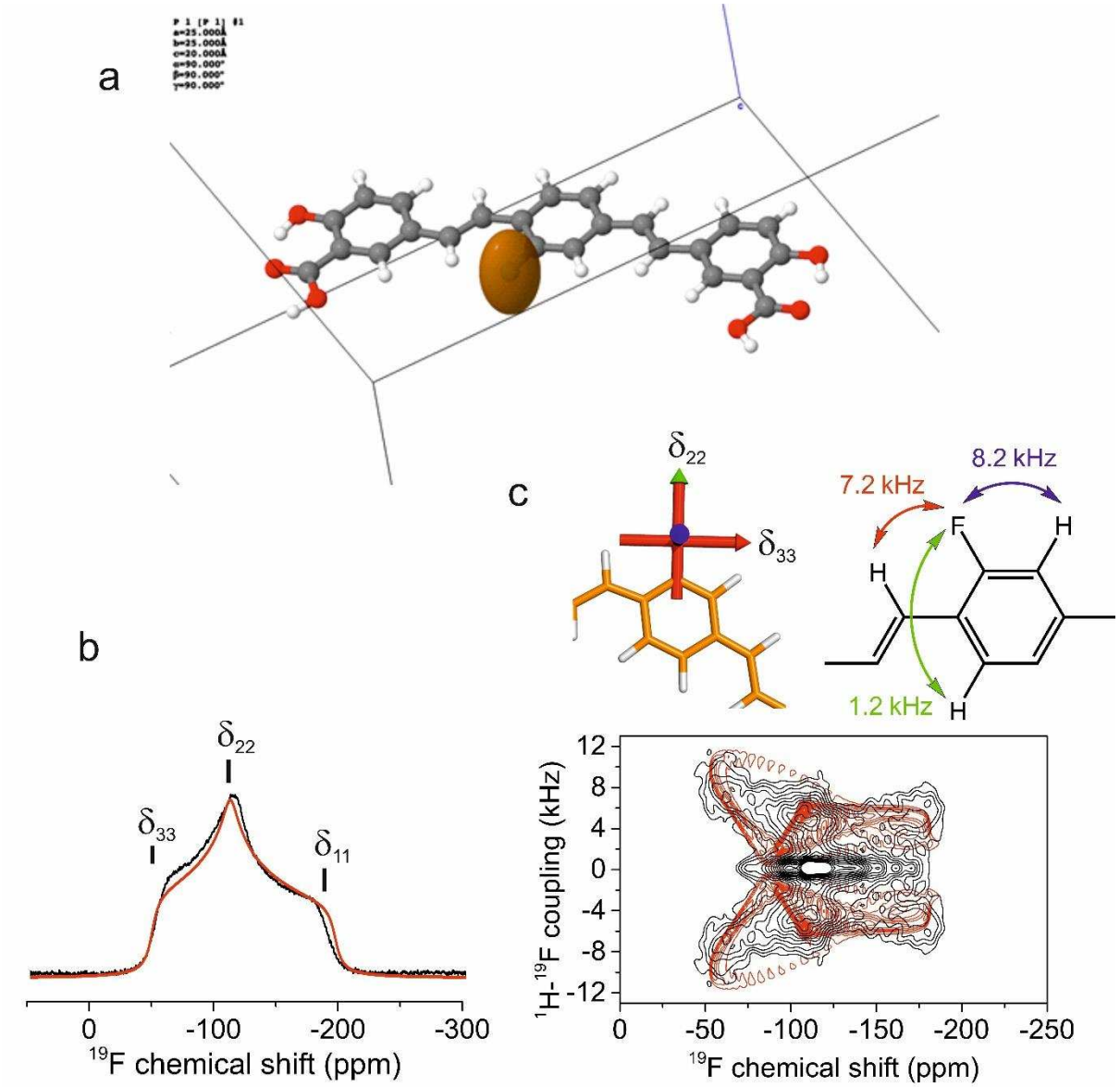

Figure S5. Measured and predicted ^{19}F chemical shift tensor values of FSB measured from ^{19}F spectra of the non-crystalline solid. (a) Optimised, lowest energy conformation of FSB showing the ^{19}F tensor orientation (orange ovoid) in the molecular frame, as calculated for a single isolated molecule using CASTEP. (b) Proton-decoupled static ^{19}F powder spectrum of solid FSB showing the measured principal chemical shift values. (c) ^{1}H-^{19}F PISEMA spectrum (black) and simulated spectrum (red) for a 4-spin system (^{19}F and 3 x ^{1}H) with the ^{1}H-^{19}F dipolar coupling constants shown. Simulated spectra for other tensor orientations are shown in Figure S4.

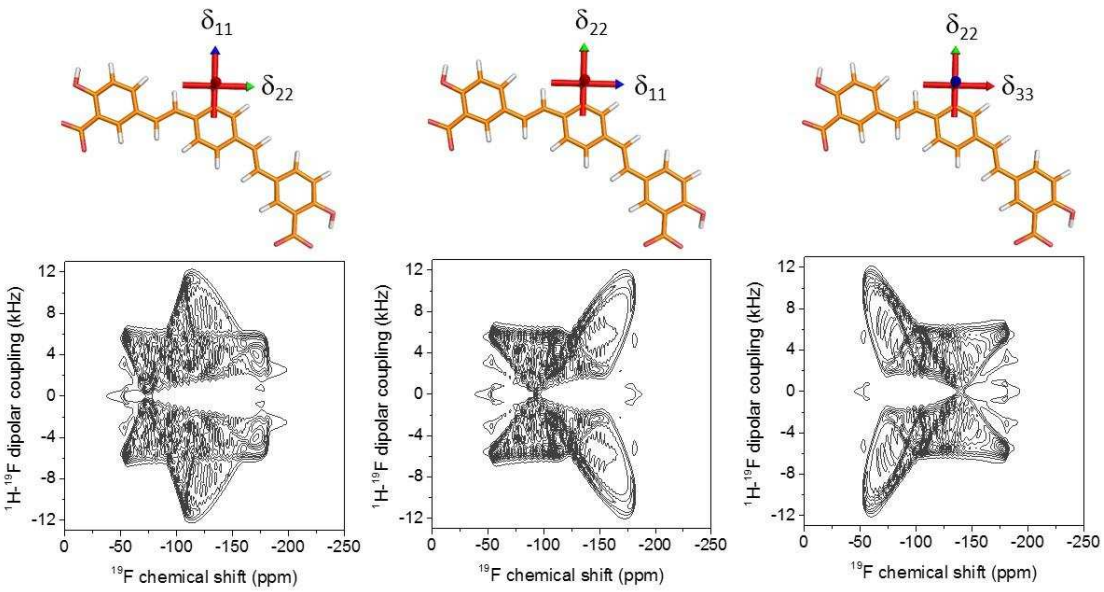

Figure S6. Simulated ^{1}H, ^{19}F-PISEMA spectra for FSB (4-spin system) in which each of the three principal axes, $\hat{\delta}_{11}$, $\hat{\delta}_{22}$ and $\hat{\delta}_{33}$, of the ^{19}F chemical shift tensor is aligned along the C-F bond. The spectrum on the right corresponds to the tensor orientation predicted by CASTEP.

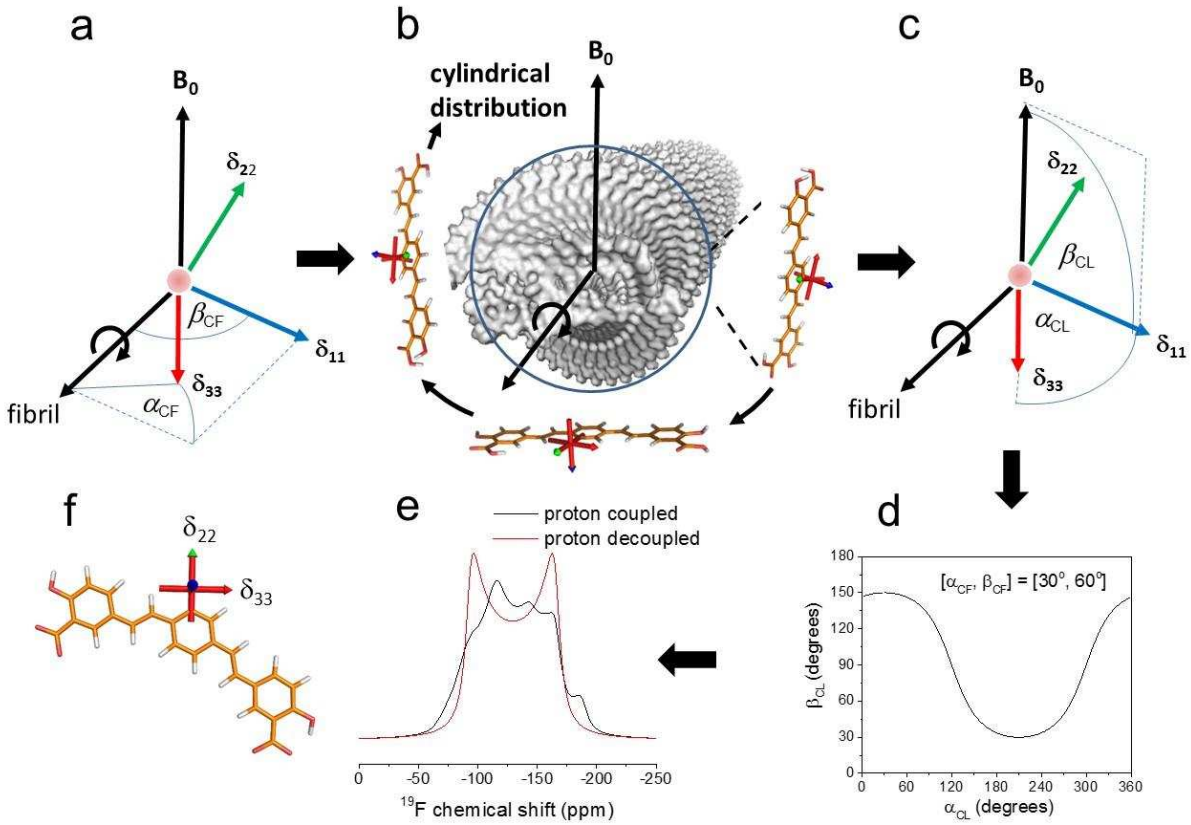

Figure S7. Stepwise procedure for simulating ^{19}F NMR spectra for FSB bound to macroscopically aligned amyloid fibrils. Steps (a-c): See main text for details. (d) The distribution of α_{CL},β_{CL} values for an arbitrary [α_{CF}, β_{CF}] combination of [30°, 60°] . (e) Simulated ^{19}F NMR spectra for the angle combination in (d). The proton-coupled spectrum includes dipolar contributions from four neighbouring ^{1}H spins illustrated in Figure S5c. (f) Orientation of the principal axes of the ^{19}F chemical shift tensor in the FSB molecule.

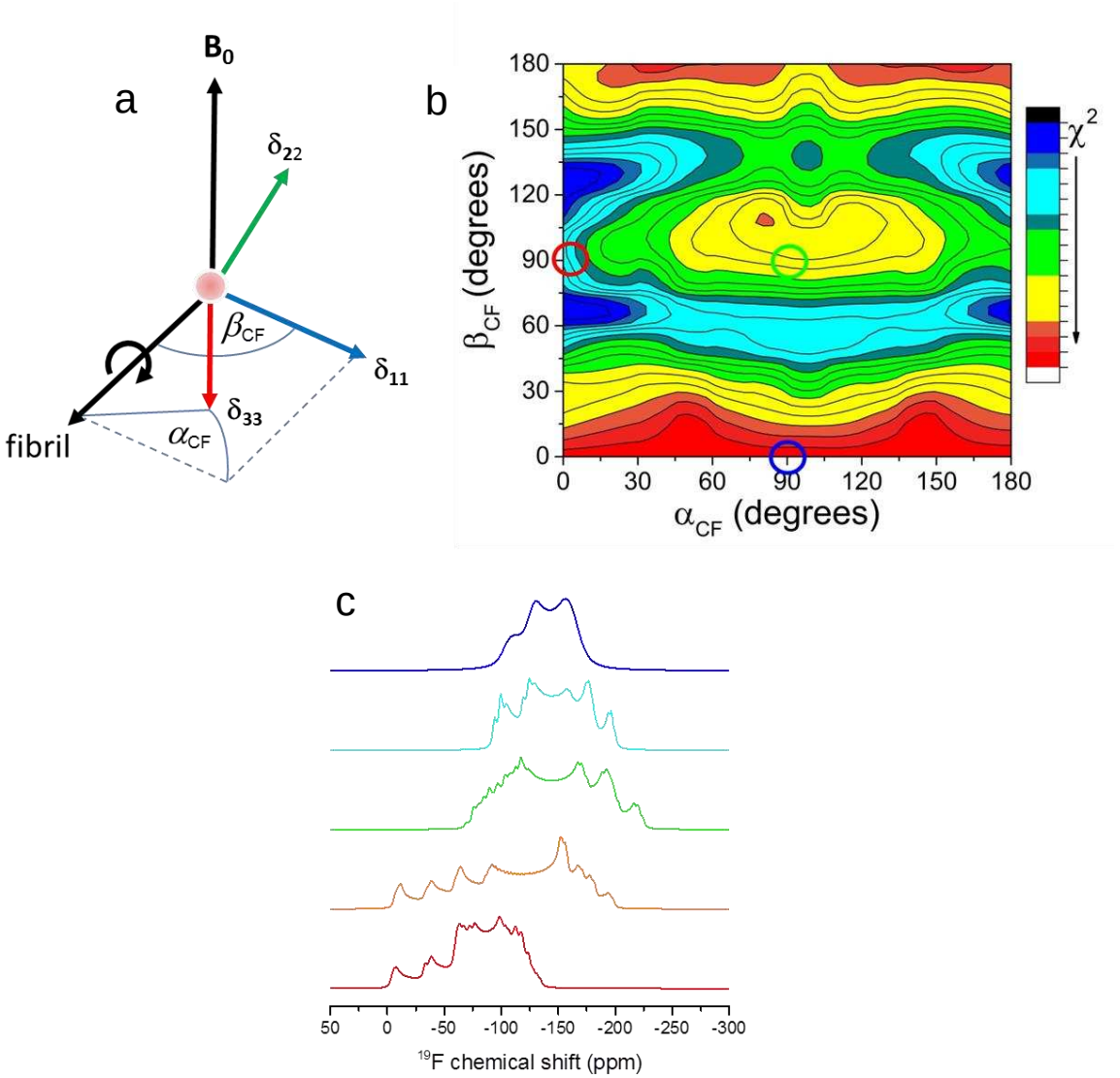

Figure S8. Simulations of ^{19}F NMR line shapes for FSB bound to oriented fibrils. (a) Definition of angles α_{CF} and β_{CF} (reproduced from Figure S5). (b) Contour plot of χ2 values representing the variance between the experimental spectrum in Figure 4b of the main text and simulated spectra for [α_{CF}, β_{CF}] combinations from [0°, 0°] to [180°, 180°] in 15° increments. The blue, red and green circles denote the an gle combinations and χ^2 values corresponding to the simulated spectra in Figure S8, for which the three principal axes, $\hat{\delta}_{11}$, $\hat{\delta}_{22}$ and $\hat{\delta}_{33}$, of the ^{19}F chemical shift tensor are aligned along the fibril axis. (c) A selection of simulated spectra colour coded according to the contour levels in (b).

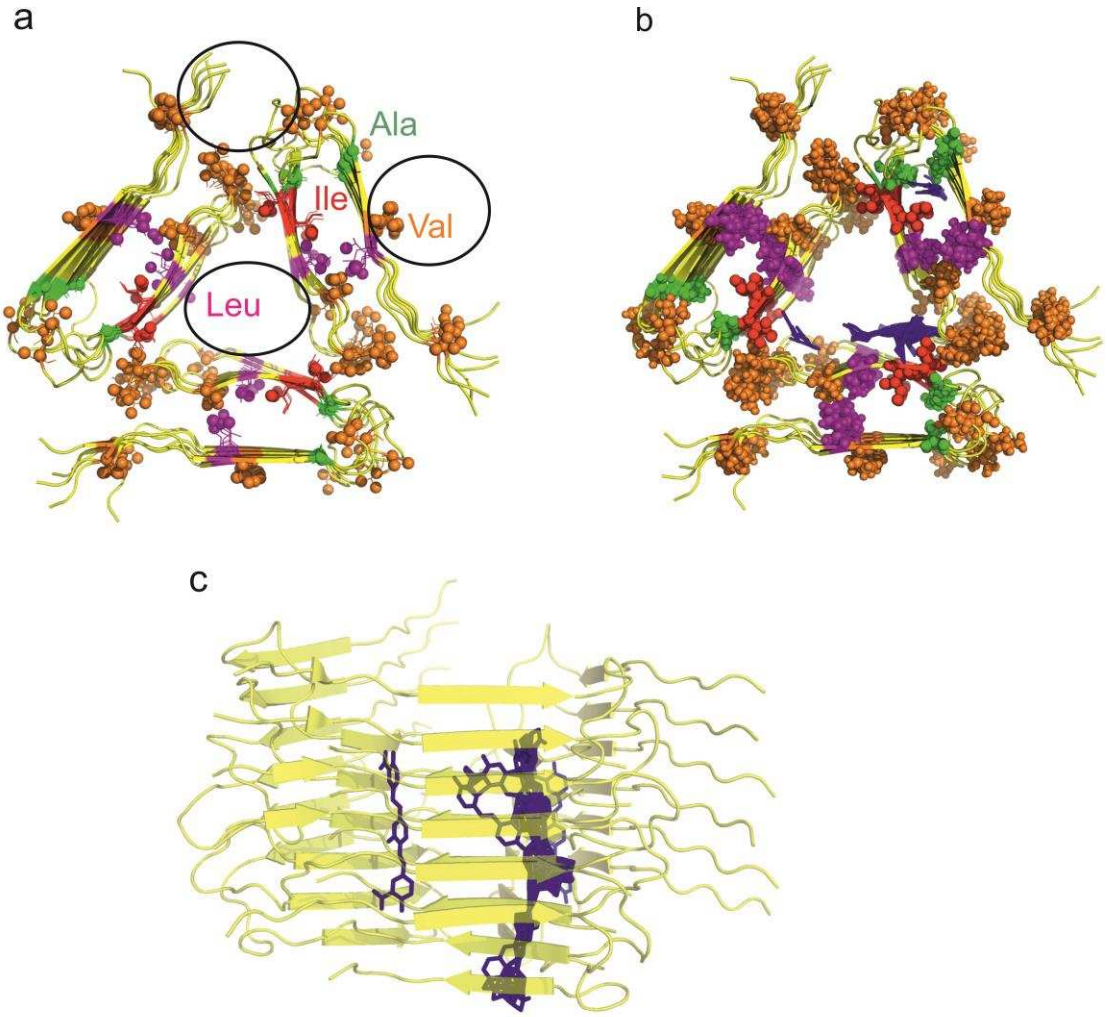

Figure S9. Molecular docking simulations. (a) Model of the three-fold (3Q) fibril arrangement of Aβ40 (from PDB file 2LMP) used in the molecular docking simulations. Circles indicate possible FSB binding sites enabling close contact with amino acids (Ala, Ile, Leu and Val) detected in the REDOR experiment, which were used to position the FSB ligand at the beginning of the docking analysis. Apart from the initial placement of ligand within the centers of the circles, no restraints were placed on the movement of the ligand during docking. (b) Final docking positions of FSB (blue) showing the proximity of Ala (green), Ile (red), Leu (magenta) and Val (orange) residues to the ligand. (c) Alternative representation of the fibril-ligand model showing the longitudinal orientation of FSB with respect to the fibril axis.

4. Supplementary references

1. Walsh, D. M.; Thulin, E.; Minogue, A. M.; Gustavsson, N.; Pang, E.; Teplow, D. B.; Linse, S., A facile method for expression and purification of the Alzheimer's disease-associated amyloid beta-peptide. FEBS J. **2009,** 276 (5), 1266-1281.
2. Stewart, K. L.; Hughes, E.; Yates, E. A.; Huang, T. Y.; Lima, M. A.; Rudd, T. R.; Guerrini, M.; Hung, S. C.; Radford, S. E.; Middleton, D. A., Atomic details of the interactions of glycosaminoglycans with amyloid-beta fibrils. J. Am. Chem. Soc. **2016,** 138 (27), 8328-8331.
3. Madine, J.; Pandya, M. J.; Hicks, M. R.; Rodger, A.; Yates, E. A.; Radford, S. E.; Middleton, D. A., Site-specific identification of an A-beta fibril-heparin interaction site by using solid-state NMR spectroscopy. Angew. Chemie. Int. Ed. **2012,** 51 (52), 13140-13143.
4. Paravastu, A. K.; Leapman, R. D.; Yau, W. M.; Tycko, R., Molecular structural basis for polymorphism in Alzheimer's beta-amyloid fibrils. Proc. Natl. Acad. Sci. USA **2008,** 105 (47), 18349-18354.
5. Fung, B. M.; Khitrin, A. K.; Ermolaev, K., An improved broadband decoupling sequence for liquid crystals and solids. J. Magn. Reson. **2000,** 142 (1), 97-101.
6. Wu, C. H.; Ramamoorthy, A.; Opella, S. J., HIGH-RESOLUTION HETERONUCLEAR DIPOLAR SOLID-STATE NMR-SPECTROSCOPY. J. Magn. Reson., Ser A **1994,** 109 (2), 270-272.
7. Bendall, M. R.; Gordon, R. E., DEPTH AND REFOCUSING PULSES DESIGNED FOR MULTIPULSE NMR WITH SURFACE COILS. J. Magn. Reson. **1983,** 53 (3), 365-385.
8. Segall, M. D.; Lindan, P. J. D.; Probert, M. J.; Pickard, C. J.; Hasnip, P. J.; Clark, S. J.; Payne, M. C., First-principles simulation: ideas, illustrations and the CASTEP code. Journal of Physics-Condensed Matter **2002,** 14 (11), 2717-2744.
9. Pickard, C. J.; Mauri, F., All-electron magnetic response with pseudopotentials: NMR chemical shifts. Physical Review B **2001,** 63 (24).
10. Perdew, J. P.; Burke, K.; Ernzerhof, M., Generalized gradient approximation made simple. Phys. Rev. Lett. **1996,** 77 (18), 3865-3868.
11. Yates, J. R.; Pickard, C. J.; Mauri, F., Calculation of NMR chemical shifts for extended systems using ultrasoft pseudopotentials. Physical Review B **2007,** 76 (2).
12. Grimme, S., Semiempirical GGA-type density functional constructed with a long-range dispersion correction. J. Comput. Chem. **2006,** 27 (15), 1787-1799.
13. Hughes, E.; Griffin, J. G.; Coogan, M. P.; Middleton, D. A., PCCP **2018,** 20, 18207-18215.
14. Bak, M.; Rasmussen, J. T.; Nielsen, N. C., SIMPSON: A general simulation program for solid-state NMR spectroscopy. J. Magn. Reson. **2000,** 147 (2), 296-330.